Association of Helical β-Peptides and their Aggregation Behavior from the Potential of Mean Force in Explicit Solvent

Clark A. Miller,[†] Samuel H. Gellman,[‡] Nicholas L. Abbott,[†] and Juan J. de Pablo[†*]
[†]Department of Chemical and Biological Engineering, and [‡]Department of Chemistry, University of Wisconsin-Madison, Madison, Wisconsin

ABSTRACT Helical β-peptides have been shown to fold into well-defined structures. In aqueous solution, some β-peptides self-assemble into nanoscale fibers, aggregates, and liquid crystalline phases. Molecular simulations, at an atomistic level, are used to examine, in a systematic manner, the interactions between distinct β-peptide molecules. The relationship between side-chain chemistry (and position along the backbone) and, in particular, aggregation behaviors, is assessed by calculating the potential of mean force or dimerization free energy of two peptides in explicit water. The free energy profiles as a function of separation for helical, amphiphilic β-peptides are consistent with experimental observations, and help explain the origins of aggregate or fiber formation in solution. Close examination of the energetic and entropic contributions to the free energy reveals that, depending on the position of certain side groups along the molecule, the tendency of two peptides to aggregate can be driven by entropy or by energy, respectively. In contrast to findings from previous works that employed a coarse representation of the solvent, it is shown that water-peptide interactions play key roles in the association behavior of β-peptides.

INTRODUCTION

There is considerable interest in understanding protein aggregation both in vivo and in vitro. Protein aggregation has been associated with a number of diseases (including Alzheimer's, Huntington's, and diabetes). In the pharmaceutical industry, protein aggregation can lead to a number of processing and therapeutic issues. Synthetic β-peptides represent a particularly intriguing class of molecules for fundamental studies of protein association. Because they are oligomers of β-amino acids, β-peptides offer considerable control over the secondary structure (1–5). By resorting to particular side chains (e.g., cyclic groups), one can confer considerable stability to the folded structure of the molecules in aqueous solution, thereby enabling association studies in which a folded structure is preserved and the aggregation process is not marred by complex unfolding events. In addition, by altering the sequence of hydrophilic and hydrophobic groups along the molecule, one can examine in a systematic manner the role of distinct forces in the aggregation of oligopeptides in solution.

A limited subset of the experimental literature on β-peptides has begun to examine their propensity to self-assemble (6–15). In an early study, cyclic β-peptides were synthesized to form nanotubes that acted as artificial ion channels (6). It was suggested that the electric dipole moment of these nanotubes could play a role in the voltage and gating mechanisms for these artificial channels. Later, a 10-residue amphiphilic β-peptide was shown to form small aggregates in solution by analytical ultracentrifugation (7). A more recent study has identified the formation of fibrils by a nonhelical β-peptide (8); in contrast, helical β-peptides have been found to form helical bundles (9,10). One of these studies observed the formation of spheres and membranes and attributed the self-assembly to hydrophobic interactions (10). Qiu et al. (11) and Daniels et al. (12) have synthesized β-peptides that display specific aggregation characteristics; their crystal structure is consistent with a bundle of eight β-peptides with buried β^3-homoleucine side chains (12). Taken together, these studies serve to illustrate the complexity that can emerge from simple alterations to relatively small molecules, and the possibilities offered by β-peptides in fundamental studies of self-assembly and protein aggregation.

A recent experimental study showed that four, sequentially similar helical β-peptides, in fact exhibit quite different aggregation behaviors (13,15). The particular β-peptides considered in that work were 10-residues long. Three of the residues were hydrophilic. Their sequences were

1a: (β^3-hTyr)-[ACHC-ACHC-(β^3-hLys)]$_3$;
1b: (β^3-hTyr)-[ACHC-ACHC-(β^3-hLys)]-[ACHC-(β^3-hLys)-ACHC]-[(β^3-hLys)-ACHC-ACHC];
2a: (β^3-hTyr)-[ACHC-(β^3-hPhe)-(β^3-hLys)]$_3$; and
2b: (β^3-hTyr)-[(β^3-hLys)-(β^3-hPhe)-ACHC]-[(β^3-hPhe)-(β^3-hLys)-ACHC]-[ACHC-(β^3-hPhe)-(β^3-hLys)].

Here, the abbreviations refer to proteinogenic side chains with β^3-hTyr = β^3-homotyrosine, β^3-hLys = β^3-homolysine, and β^3-hPhe = β^3-homophenylalanine. The ACHC refers to *trans*-2-aminocyclohexanecarboxylic acid. The corresponding chemical structures and diagrams of side-chain presentation are given in Fig. 1. Peptides **1a** and **2a** were designed with the hydrophilic residues on one face of the helix, whereas peptides **1b** and **2b** were designed with the hydrophilic residues distributed on each of the three faces. The formation of higher-order structure was assessed by examining the emergence of liquid crystalline behavior. In the case of **1a**,

Submitted September 9, 2008, and accepted for publication November 24, 2008.

*Correspondence: depablo@engr.wisc.edu

Editor: Gregory A. Voth.

0006-3495/09/06/4349/14 $2.00

doi: 10.1016/j.bpj.2008.11.076

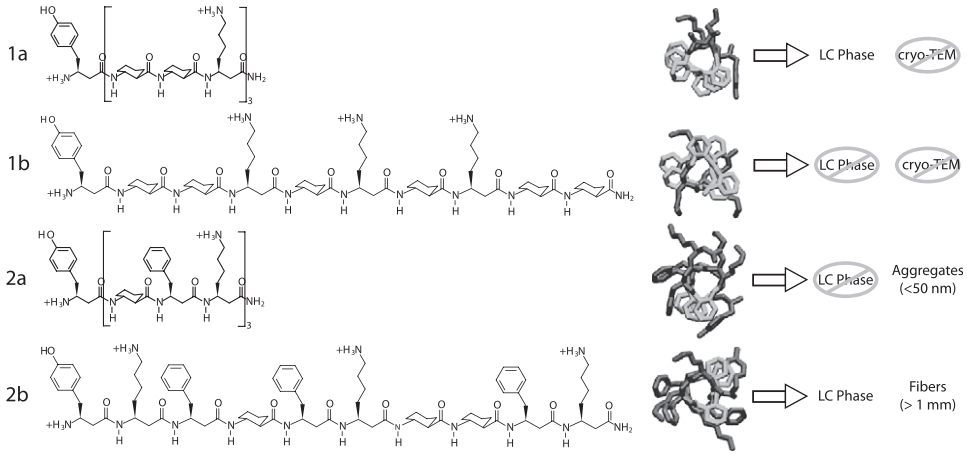

FIGURE 1 Structures and stick representations of the β-peptides considered in this work. The side chains are colored with the cyclic (ACHC) residues in green, the β^3-homolysine residues in blue, the β^3-homotyrosine residue in red, and the β^3-homophenylalanine residues in purple. For clarity, hydrogens have been removed. Stick representations were made using VMD (61). Also included is a summary of the experimental work on higher order structures (13,15).

a lyotropic liquid crystalline phase was observed at 10 wt % (13). Peptide **1b** was not observed to form a liquid crystalline phase (13). Because of the difference in facial display of hydrophilic residues between **1a** and **1b**, it was proposed that in the case of **1a**, hydrophobic forces drive the aggregation of individual peptides into higher order structures, which then formed a liquid crystalline phase. In a follow-up study (15), peptides **2a** and **2b** were studied for liquid crystalline behavior. Peptide **2a** did not form a liquid crystalline phase (up to 15 wt %), whereas **2b** did at 10 wt % (15). These observations suggested that something more than hydrophobic-driven assembly was at work in these molecules. Also in that study, the structures formed by **2a** and **2b** were observed by cryo-transmission electron microscopy (TEM) and small-angle x-ray scattering (15). It was reported that **2a** formed small aggregates (radius $<$50 nm) at 8 wt %, and that **2b** formed long fibers (length >1 μm). The experimental observations described in this paragraph are summarized in Fig. 1. The ability to form a variety of assembled structures in solution resulting from small changes in primary sequence emphasizes the need to develop molecular models capable of describing the assembly process.

Past computational work on β-peptides has mainly focused on the folded structure of individual molecules that arises for a given sequence of amino acids (16–21). In a previous report (22), we examined the thermal and mechanical stability of helical β-peptides using expanded ensemble density of states and molecular dynamics simulations. We found that torsional and electrostatic interactions are largely responsible for the mechanical stability of β-peptides. In a more recent study (23), we analyzed the mechanical stability of β-peptides in both explicit and implicit solvent models. It was shown that although both the explicit and implicit solvent models lead to similar helical structures, the use of an approximate implicit solvent model exacerbates the resistance to mechanical deformation. In contrast, the explicit solvent treatment is successful at capturing the energetic and entropic contributions to peptide stability, as well as the intriguing temperature dependence of some of the peptide's mechanical stability.

Few computational studies have attempted to examine the self-association of β-peptides. Recently, we presented a study of the aggregation of collections of β-peptide molecules using a multiscale approach (24). The free energy between two peptides was determined using atomistic simulations, and a coarse-grained model was developed that matched the free energy profile of the atomistic model. Electrostatic interactions, in particular the helical dipole moment, were found to be an important contributing factor in the self-assembly process. However, the solvent was treated implicitly. In light of the importance that hydrophobic forces may play in the self-association of β-peptides, it is of interest to perform the atomistic simulations in explicit water. In a series of works by Martinek et al. (8,10) and Hetényi et al. (9), ab initio and molecular dynamics simulations were used to show that those β-peptides that form fibrils or membranelike structures in experiment are also stable over 3-ns trajectories in computer models of those structures. The molecular dynamics simulations from the literature (8–10) were performed in water, with β-peptides made entirely of cyclic residues. However, they did not examine the effects of side chains (and sequence) on the assembly of β-peptides.

Peptide association can be investigated by determining the potential of mean force (PMF) between two peptides. It is of interest to point out that this quantity has been calculated before for α-peptides (25–27). Curtis et al. (25) used Monte Carlo simulations and an implicit solvent model to examine the PMF between two polyalanine and two polylysine α-peptides. Soto et al. (26) used replica exchange molecular dynamics simulations to determine the PMF of polyalanine (decamer) in cyclohexane at multiple temperatures. These authors reported the existence of both β-sheet and α-helical dimers. Electrostatic (dipole-dipole) interactions were found to stabilize side-by-side antiparallel α-helical dimers. MacCallum et al. (27) used molecular dynamics simulations in explicit water to determine the PMF between two polyalanine and two polyleucine α-peptides (20-mers), but did so with a fixed orientation. They found a large unfavorable enthalpic cost and favorable increase in entropy that led to

the hydrophobic association of the α-helices. They also found a decrease in peptide-peptide energy, increase in peptide-water energy, and decrease in water-water energy upon association.

In this work, we determine how amino-acid sequence and side-chain selection affect the assembly of β-peptides, and do so with an explicit solvent representation. We examine the self-assembly of β-peptides **1a**, **1b**, **2a**, and **2b** by determining the PMF between two peptides, and we use our results to interpret available experimental evidence for aggregation of these four peptides. In the sections that follow, we describe the simulation model and the methods used to determine the PMF. We then present the results of our calculations and discuss them in the context of recent experimental observations.

MODEL AND METHODS

Molecular model

For our studies we consider proteinogenic amino acids and use their common abbreviations (as in (1,2)). The side chains for the β-peptides considered in this work are substituted on the β-carbon, but we also consider cyclically constrained residues, formed from ACHC (Fig. 1). One of the desirable attributes of β-peptides is that different types of helices can be designed by changing the residues involved and their sequence (1). The helices are named according to the hydrogen bonding between N–H and C=O. For example, a 14-helix has 14 atoms between the hydrogen bond of atoms C=O(i) and H-N(i-2). The ACHC residue has been shown experimentally (28,29) and theoretically (22) to stabilize the 14-helix. In experiments and simulations, each of the four peptides forms a stable 14-helix (13,15,23). The structures of the four peptides are shown in Fig. 1.

The CHARMM27 (30,31) all-atom force field is used to model these β-peptides. Note, however, that the CHARMM force field does not include all the parameters necessary for β-peptides. The parameters for peptides **1** and **2** are the same as in our previous study (23) and are included as Supporting Material.

The potential energy function employed in this work is of the form $U = U(r_{ij}, b, \psi, n, \phi, \omega)$, where $r_{ij} = |\mathbf{x}_j - \mathbf{x}_i|$ is the distance between site i and j; $\mathbf{x}_i$ are the Cartesian coordinates of site i; b is the bond length between connected sites; ψ is the angle between successive bonds; ϕ is the dihedral angle; n is the multiplicity of the dihedral angle; and ω is the improper dihedral angle (30,31). The potential energy is then defined by

$$\begin{aligned} U = & \sum_{i,j}^{N^2} \varepsilon_{ij}\left[\left(\frac{\sigma_{ij}}{r_{ij}}\right)^{12} - 2\left(\frac{\sigma_{ij}}{r_{ij}}\right)^{6}\right] \\ & + \sum_{\text{Coulombic}} \frac{1}{4\pi\varepsilon_o}\frac{q_i q_j}{r_{ij}} + \sum_{\text{bonds}} k_b(b-b_0)^2 \\ & + \sum_{\text{angles}} k_\psi(\psi-\psi_0)^2 + \sum_{\text{dihedrals}} k_\phi\left[1+(cos(n\phi-\phi_0))\right] \\ & + \sum_{\text{impropers}} k_\omega(\omega-\omega_0)^2 \end{aligned} \qquad (1)$$

The first summation represents the Lennard-Jones interaction between sites, N is the number of sites, ε_{ij} is the Lennard-Jones well-depth, and σ_{ij} is the position of the minimum in the potential. The second summation accounts for the electrostatic (Coulombic) energy between sites, where q_i is the charge of site i, and ε_o is the vacuum permittivity. The other summations correspond to the bond energy between connected sites, the angle energy between successive bonds, the dihedral energy, and the improper dihedral energy. The corresponding constants, k_b, k_ψ, k_ϕ, and k_ω, and the value for the location of the minimum energy, b_0, ψ_0, ϕ_0, and ω_0 are described in the literature (32,33). In addition, a 1–3 exclusion principle was used for nonbonded interactions and the 1–4 Coulombic interactions were scaled by 0.4, consistent with the CHARMM force field (30).

Molecular dynamics simulations were performed using the GROMACS (34–36) simulation package. The TIP3P model (37) of water was selected for explicit solvent simulations to be compatible with the CHARMM force field. Lennard-Jones interactions were truncated with a twin-range scheme at 1.0 and 1.5 nm. The electrostatic interactions were calculated using a particle-mesh Ewald technique (38) with a short-range cutoff of 1.0 nm, a maximum relative error of 10^{-5}, and a fourth-order spline. The peptides were simulated with each β^3-homolysine and the N-terminus protonated. To counter the positive charge of each peptide (with a net charge of +4), chloride ions were included in the simulation cell. We used 3000 water molecules and a cubic box with a length ~4.4 nm. Larger system sizes were also considered for **1a** and **2b** with 4870 and 4851 water molecules and rectangular boxes of ≈4 nm × 4 nm × 8 nm. Molecular dynamics simulations were first performed at constant pressure (1 bar) and temperature (300 K) using the Berendsen method (39) for a brief equilibration period (<1 ns). The thermostat had a coupling of 0.2 ps and the barostat had a coupling of 0.1 ps and a compressibility of 0.45×10^{-4} bar. The bonds were constrained to equilibrium lengths using SETTLE (40) for water and LINCS (41) for all other bonds and a time step of 0.002 ps was used. Production simulations were run in the NVT ensemble for 5 ns and the properties were averaged over at least 4.5 ns. Longer simulations of 10 ns were also performed for peptides **1a** and **2b** with properties averaged over the last 9 ns.

The helicity of the peptide was calculated from the dihedral angles ϕ (C(=O)-N-C_β-C_α) and ψ (C_β-C_α-C(=O)-N) using the expression

$$H_{\text{dih}} = \frac{\sum_{\phi,\psi} H_\phi H_\psi}{N_{\phi,\psi}}, \qquad (2)$$

where $N_{\phi,\psi}$ is the number of ϕ- or ψ-angles. H_ϕ is defined as

$$H_\phi = \begin{cases} 1 & \text{if} \quad |\phi-\phi_o| \le a \\ 1 - \frac{|\phi-\phi_o|-a}{b-a} & \text{if} \quad a < |\phi-\phi_o| \le b \\ 0 & \text{if} \quad |\phi-\phi_o| > b \end{cases}, \qquad (3)$$

and a similar definition was used for H_ψ. The parameters a, b, ϕ_o, and ψ_o depend on the type of helix. For the 14-helix $a = 20$, $b = 39$, $\phi_o = -135$, and $\psi_o = -140$, whereas for the 12-helix $a = 20$, $b = 39$, $\phi_o = 95$, and $\psi_o = 103$.

We also determined the overall potential energy and its various contributions, such as Lennard-Jones or electrostatic energies. The end-to-end distance (Fig. 2) was defined as the distance from the nitrogen of the amino group on the second residue from the N-terminus to the carbon of the carbonyl group on the second residue from the C-terminus. The end-to-end distance was defined in that manner because the first and last residues are more likely to fluctuate from the folded state. The orientation between the two peptides ($\cos(\theta_1)$) was determined by analyzing the dot product between the two end-to-end vectors. When $\cos(\theta_1) = 1$, the peptides are parallel and when $\cos(\theta_1) = -1$, they are antiparallel. A second orientation vector ($\cos(\theta_2)$) is determined by analyzing the dot product between the end-to-end vector of the first peptide with the separation vector. When $\cos(\theta_2) = 0$, the peptides are side-by-side and when $\cos(\theta_2) = 1$, the peptides are aligned end-to-end.

Potential of mean force

The PMF represents the reversible work required to arrive at any point along a chosen reaction coordinate ξ. In this study, the reaction coordinate is defined as the distance between the C_α carbon of the fifth residue between two peptides, ξ (Fig. 2). For this reaction coordinate, the PMF, $w(\xi)$, represents the free energy of aggregation between two molecules.

Several methods are available to calculate the PMF, including umbrella sampling (42), the constraint-force method (43), and the stochastic expanded-ensemble density-of-states method (44). A recent summary and

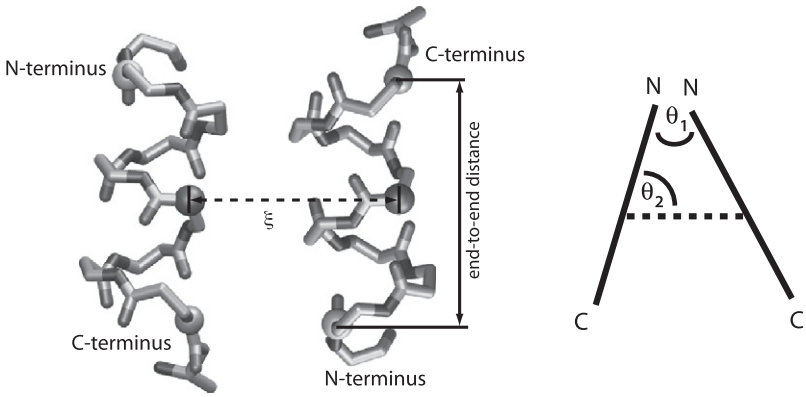

FIGURE 2 The reaction coordinate and end-to-end distance used in this article. The backbone is shown as sticks and the spheres represent the atoms used to define the reaction coordinates. The end-to-end distance is defined as the separation between the nitrogen on the N-terminus and the carbonyl carbon of the C-terminus. The reaction coordinate, ξ, is defined as the distance between the C_α carbons of the fifth residue for each residue.

comparison of methods to determine the PMF using molecular dynamics showed that calculating the PMF from the so-called constraint-force method (see below) gives good results (43). One can obtain the PMF by integrating over the force

$$w(\xi) = \int_{\xi_0}^{\xi} \langle f(r') \rangle_{r'} dr' + 2k_B T \, ln(\xi/\xi_0) + C, \quad (4)$$

where w is the PMF; ξ is the reaction coordinate; $\langle f(r') \rangle_{r'}$ is the mean force at a particular value of separation; k_B is Boltzmann's constant; T is the temperature; and C is a constant of integration. This constant can be chosen to match a reference value for w. In this work, the largest separation is given a reference value of zero. The simulations are run by constraining the reaction coordinate to a specific value and monitoring the force required to constrain the simulation to that value. After performing the simulation at several values of the reaction coordinate, one can integrate Eq. 4 to arrive at w. The simulations are run in the NVT ensemble at 300 K. For rectangular boxes, the peptides are restricted to move along the longest dimension (z) of the box by applying harmonic restraints in the x and y direction on the C_α carbon of the fifth residue.

Replica-exchange molecular dynamics simulations

Replica exchange molecular dynamics simulations (45–49) were performed to assess the effects of temperature on association. Using a parallel version of the GROMACS simulation software, 13 replicas were spaced every 5° between 270 and 330 K. The simulations were performed in the NVT ensemble for 10 ns while exchanges were proposed every 100 time steps. All other parameters were the same as described above for molecular dynamics simulations.

RESULTS AND DISCUSSION

The PMFs of the four peptides considered in this work are shown in Fig. 3. The results are consistent with previous experimental evidence of peptide association, as will be discussed. We also characterized the orientation between the two peptides as described above and those results are given in Fig. 4.

The PMF of peptide **1a** exhibits a local minimum near $\xi = 0.75$ nm of ~2 k_BT. Although the rest of the curve is generally repulsive, this free energy profile could be consistent with the formation of higher-order structures. In experiments, peptide **1a** forms a liquid crystalline phase (13), although the exact nature and underlying structure of those phases is unclear. Aggregation of **1a** was also observed by analytical ultracentrifugation (7) experiments in which the monomer was shown to be in equilibrium with a tetramer. Although

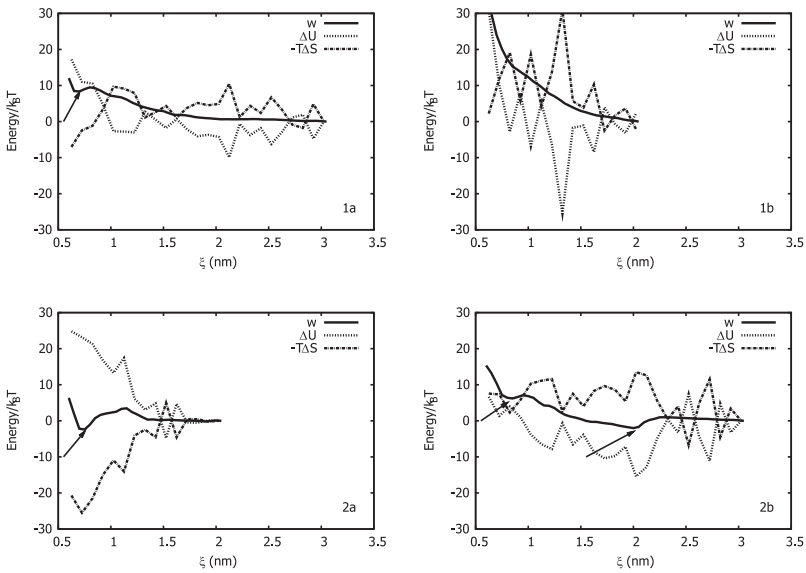

FIGURE 3 The contributions to the PMF between two peptides as a function of peptide separation.

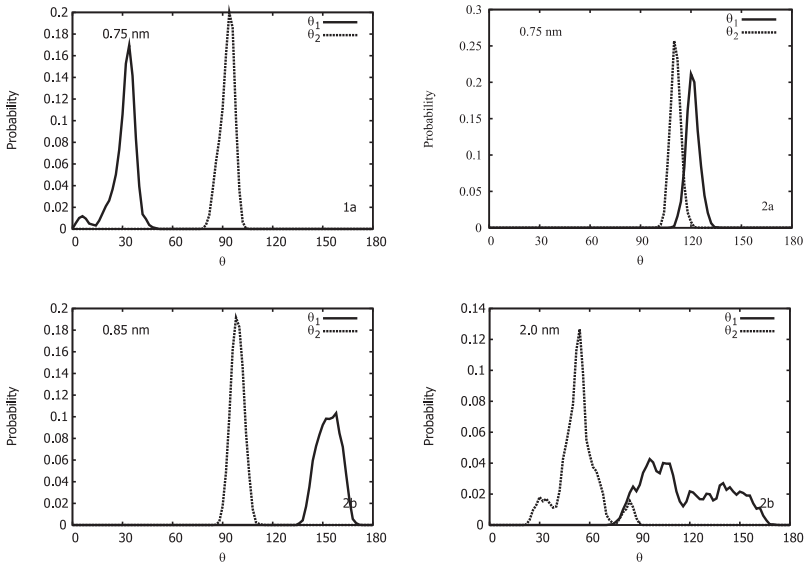

FIGURE 4 The probability distribution of orientations between two peptides at the minima in the PMF in Fig. 3. Shown is the **1a** at 0.75 nm, **2a** at 0.75 nm, and **2b** at 0.85 nm and 2.0 nm.

the PMF in Fig. 3 corresponds to the free energy of dimer formation in dilute solution, at higher concentrations the peptide could conceivably associate into tetramers or larger multimeric structures. Examination of the orientation between the two peptides provides some insights into plausible higher order structure. Fig. 4 shows the probability distribution of the angles at the local minimum of the free energy ($\xi = 0.75$ nm). From the dot product of the end-to-end vectors, $\cos(\theta_1)$, the angle is between 0° and 40°, indicating that the peptide helices adopt a parallel orientation. The dot product of the end-to-end and separation vectors, $\cos(\theta_2)$, adopts an angle close to 90°, indicative of a side-by-side configuration. Both parallel and antiparallel helical orientations were found in the crystal structure of a bundle of eight helical β-peptides (12). The observation here of a parallel arrangement is consistent with this structure. A snapshot of the peptide in this orientation is presented in Fig. 5. It shows the two peptides arranged side-by-side with their hydrophobic faces pointed toward each other.

A rearrangement of the hydrophilic β^3-homolysine residues leads to peptide **1b**. The PMF is repulsive at all separations considered here. Experiments indicate that peptide **1b** does not exhibit a liquid crystalline phase (13) or any tendency to aggregate. The PMF shown in Fig. 3 is consistent with that observation.

The PMF for peptide **2a** exhibits a minimum of 4 k_BT at 0.75 nm. Examination of the relative orientation of the molecules shows that at this separation (Fig. 4), the peptides are oriented at an angle of $\theta_1 \approx 120°$ and side-by-side ($\theta_2 \approx 110°$), in a manner that buries the hydrophobic residues and shields them from the solvent. In this case, the peptides are not perfectly antiparallel, but adopt a specific angle (Fig. 5). Again, the antiparallel helical orientation is consistent with what has been observed in a crystal structure of a bundle of eight β-peptides (12). Experiments on peptide **2a** did not provide evidence of liquid crystalline behavior, but TEM images did reveal the formation of small aggregates (15). The small aggregates are consistent with the minimum in the PMF and the strong tendency for side-by-side orientation observed in our simulations. It is interesting to make a comparison of this peptide with its analog **1a**, which has six ACHC residues compared with the three ACHC and three β^3-hPhe residues of **2a**. Both exhibit shallow minima (of a few k_BT) that correspond to a side-by-side orientation. But subtle differences between the two arise from the substitution of three ACHC residues with β^3-hPhe. First, the

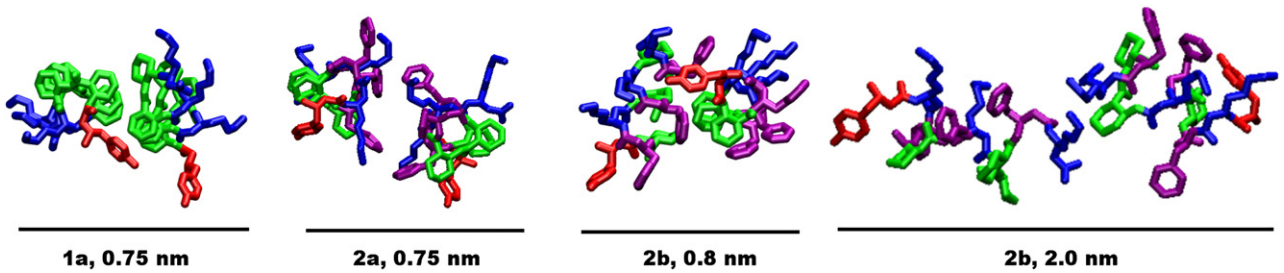

FIGURE 5 Stick representations of β-peptides **1a**, **2a**, and **2b** at the free energy minima. The figures are colored with the cyclic (ACHC) residues in green, the β^3-homolysine residues in blue, the β^3-homotyrosine residue in red, and the β^3-homophenyalanine residues in purple. For clarity, hydrogens have been removed. These figures were made using VMD (61).

minimum of **2a** is a global, deeper minimum, compared with the slight local minimum of **1a**; the minimum is twice as deep in the case of **2a**. Second, the orientation at the minimum position of **2a** deviates more from the antiparallel helical arrangement than that in **1a**.

The PMF corresponding to peptide **2b** exhibits two minima at ~0.8 and 2 nm, each with a depth of a few k_BT. The first minimum at 0.8 nm is local, and appears to be similar in many respects to the side-by-side minimum of peptides **1a** and **2a**. Fig. 4 shows that at close separations the peptide end-to-end vectors are antiparallel ($\theta_1 \approx 150^\circ$) and in a side-by-side orientation ($\theta_2 \approx 90^\circ$). For the global minimum near 2 nm, the peptides are also antiparallel, but exhibit a broader distribution ($\theta_1 \approx 90^\circ$–$160^\circ$). The end-to-end and separation vectors adopt an orientation ranging from side-by-side ($\theta_2 \approx 90^\circ$) to end-to-end ($\theta_2 \approx 30^\circ$). A representative configuration shown in Fig. 5 shows these two peptides at a separation of 2 nm. These snapshots show how, at short separations, the peptides align side-by-side, whereas at larger separations they can align in an end-to-end manner. Experiments indicate that peptide **2b** forms a liquid crystalline phase, and TEM images show that long fibers are formed at large concentrations (15). We therefore speculate that the formation of fibers observed in experiments is a result of this end-to-end association. The side-by-side association could lead to fibers of a larger diameter or inter-fiber association.

The PMFs shown in Fig. 3 for the interaction of peptides **1a**, **1b**, **2a**, and **2b** show how delicate peptide-peptide self-assembly can be. Subtle changes in the organization of the hydrophilic groups and the substitution of different hydrophobic groups can lead to diverse association phenomena. We find that the PMF results qualitatively agree with the experimental evidence and reveal what orientations can be adopted in the assembly process.

Examination of the energetic and entropic contributions to the PMF provides some insights into the mode of interaction during the formation of peptide dimers. Throughout the simulation, the potential energy is monitored and averaged for each value of the reaction coordinate. The entropic term is then calculated using the relationship $w(\xi) = \Delta U - T\Delta S$. The results are also shown in Fig. 3, where the energetic term is shown as a dashed line and the entropic term as a dotted line. The estimated error in the PMF is $<1\ k_BT$, whereas that of the energy and entropy is ~3 k_BT; thus, small variations in energy and entropy during the peptide association process are not statistically meaningful. Note, however, that the general trends observed upon association of the peptides are significant, in particular whether the entropy or energy changes are positive or negative.

The interaction between peptide **1a** molecules at short distances (<1 nm) is entropically favorable. The potential energy of interaction actually increases as two molecules are brought closely together. Near the local minimum in the PMF at $\xi = 0.8$ nm, as seen in Fig. 3, during formation of a dimer of **1a**, the entropy of the system increases enough to overcome the energetic penalty and drive the association process. The association of **1a** is consistent with a traditional hydrophobically driven assembly process, which is largely entropy-driven (50). A close examination of the conformations of the two peptides reveals that the molecules line up their hydrophobic faces and, at small separations, no water is left between them (Fig. 5). The PMF of the peptide also exhibits a small barrier that must be overcome for the molecules to find the minimum of the hydrophobically associated dimer. Barriers such as these have also been observed in the dissociation of ions in water, and the transition has been related to the rearrangement of the structure of water upon dissociation (51). In a similar manner, the water surrounding the hydrophobic groups must move from between the two peptides before the assembly can take place.

The PMF of peptide **1b** is mainly repulsive. Both the energetic and entropic terms increase as the peptides are brought together. Overall, we see an increase in energy upon association that is larger than that observed for peptide **1a**. Recall that **1b** presents a β^3-homolysine group on each face of the helix. As the two faces approach each other, the interaction between positively charged amine groups could lead to a larger repulsive energy. Overall, it is observed that peptide **1b** exhibits pronounced energy changes as the molecules are brought into proximity. At some particular separations the energy of attraction is particularly favorable (e.g., at $\xi = 1.8$ nm), but such deep minima are always accompanied by large entropic penalties that inhibit association. The central finding of this comparison is that a simple change in the presentation of hydrophilic groups can lead to the peptides being more repulsive in solution, thereby indicating how sensitive hydrophobically driven assembly can be to the presentation or orientation of hydrophilic groups.

The PMF of peptide **2a** exhibits some similarity with that of peptide **1a**. In both cases, the minimum in the PMF is found near 0.8 nm, but for peptide **2a**, it appears to be a global minimum. In contrast to peptide **1a**, however, the energetic term is increasingly repulsive as the peptides are brought together, whereas the entropic term becomes increasingly attractive. For peptide **2a,** the magnitudes of the energetic and entropic terms are larger than for **1a**, and the balance between the repulsive energetic term and the attractive entropic term leads to a deeper minimum. In this case, the association process is clearly driven by entropy and is not favored by energy.

The PMF of peptide **2b** exhibits two minima. Near the global minimum at 2 nm, the energetic term is at a minimum, whereas the entropic term is at a maximum. Our results indicate that upon scrambling the sequence of the peptide from **2a** to **2b**, the assembly process is driven by energy, and no longer by entropy (in contrast to **2a**). The energy is observed to increase again as the peptides get closer. The local minimum at 0.8 nm is barely noticeable and it corresponds to a slight minimum in the entropic term at that separation.

It is driven by entropy, and is reminiscent of that observed for peptide **1a**.

The energetic term can be further decomposed into nonbonded and bonded interactions. The bonded interactions do not change significantly along the reaction coordinate. This is a somewhat expected result, since the overall conformation of the peptides does not change significantly as the peptides are brought together. In contrast, the nonbonded interactions exhibit pronounced changes upon association. Fig. 6 shows the average Lennard-Jones and electrostatic contributions to the energy at each value of the reaction coordinate, along with the change in total potential energy. The data for peptide **1a** indicate an overall increase in the potential energy. The Lennard-Jones contribution to this term decreases with decreasing peptide separation and the Coulombic energy increases. This rise in electrostatic energy dominates the potential energy, and leads to an increase in the overall potential energy.

For peptide **1b** we find a pronounced minimum in the potential energy near 1.3 nm. This minimum is accompanied by a large decrease in the Coulombic energy and a small increase in the Lennard-Jones energy. Aside for the particular separation of 1.3 nm, the Lennard-Jones term remains largely unchanged as a function of separation, even at close peptide distances, where the Coulombic term increases appreciably.

The potential energy of peptide **2a** increases at close separations and is slightly larger than for **1a**. Both peptides exhibit increases in the Coulombic energy at close separations, but only peptide **2a** shows a small increase in the Lennard-Jones energy of the system. This appears to be a key difference in the energetics of the hydrophobic assembly of the two facially amphiphilic peptides, influencing both the energy of association and the PMF profile. Peptide **2b** is different from the others in that the potential energy exhibits a minimum near 2 nm. This potential energy profile is dominated by the Coulombic energy, particularly at large separations. At a separation of 1.3 nm, the Lennard-Jones term starts to decrease as the peptides come closer together.

For all four peptides considered here, the overall potential energy follows the same underlying trends as the Coulombic energy, and the Lennard-Jones contributions exhibit little variation with peptide separation. In previous work we have shown that the helix dipole moments of β-peptides are quite large (35–50 Debye) (24). The configurations observed at the free energy minima correspond to antiparallel side-by-side orientations or end-to-end parallel orientations. Both of these orientations are similar to those corresponding to the minimum-energy configurations of dipolar molecules. Also note that each of the four peptides has a net charge of +4, a fact that partially explains why the Coulombic energy increases as the peptides approach each other.

Role of water during association

Water plays an important role in the association of the peptides. The influence of water can be examined in more detail by looking at the nonbonded peptide-water energy, the solvent-accessible surface area (SASA), and the hydrogen bonds of the system. The nonbonded energy was decomposed into three terms: peptide one-atoms and peptide two-atoms (ΔU_{pp}); peptide and water atoms (ΔU_{pw}); and water-water atoms (ΔU_{ww}). The magnitude reported between peptide and water atoms is obtained by averaging the ΔU for peptide one-water and peptide two-water atoms. The results for each peptide are shown in Fig. 7.

Analysis of the nonbonded energy terms of peptide **1a** reveals that the energy of interaction between the peptides decreases by ~10 k_BT when they are brought together. Despite the repulsive total potential energy, the peptide-peptide contribution is favorable. In contrast, for peptides **1a**, **2a**, and **2b**, the

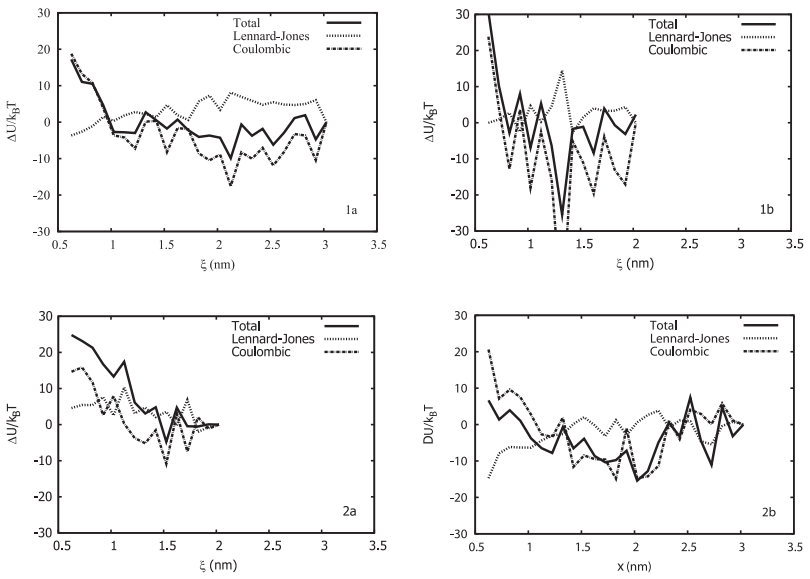

FIGURE 6 The contributions to the potential energy as a function of peptide separation.

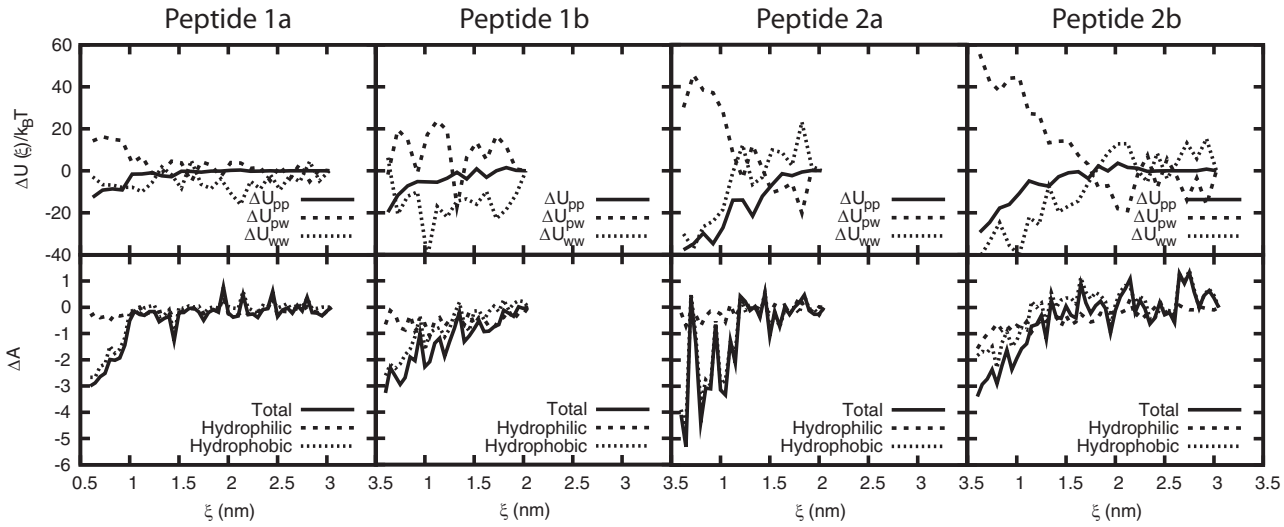

FIGURE 7 Water-peptide properties as a function of peptide separation. (*Top*) Peptide-water energies. (*Bottom*) Change in peptide SASA (ΔA).

energy between each peptide and the water increases upon association. This trend, which is particularly pronounced for peptides **2a** and **2b**, occurs because fewer water atoms are in contact with peptide atoms as the two peptides approach each other. The increase of water-peptide energy is accompanied by a decrease of water-water energy. The energy can be thought of in terms of hydrogen-bond formation. As hydrogen bonds are lost between the peptide and water, new hydrogen bonds are formed between water molecules. Note that the peptide-water energy is generally larger for peptide **2b**, and that it exhibits a drop in ΔU_{pw} near 2 nm, which corresponds to the absolute minimum in the PMF.

The results for peptide **1b** are somewhat dissimilar from those for the other peptides. The peptide-peptide energy decreases upon association, but the water-peptide interaction does not exhibit a monotonic increase as the peptides approach each other. It is interesting to note that despite the peptide-peptide attraction being more favorable for **1b** than for **1a** ($-20\ k_BT$ compared with $-10\ k_BT$), it is peptide **1a** that has been observed to aggregate. Peptide **1b** does not aggregate. This further underscores the importance of understanding the role of solvent (water) in mediating the peptide association process.

Overall, we find a decrease in ΔU_{pp} as the two peptides are brought closer. This is accompanied by a decrease in ΔU_{ww} while the peptide-water energies, ΔU_{pw}, increase. There are similarities in the general trends, but differences between each peptide arise when looking at the quantitative change in energy upon association. The strength of these interactions is an important factor in determining the change in potential energy upon association. We also note that in most cases, the magnitude of the peptide-water energy increase is larger than the magnitude of the decrease in both peptide-peptide and water-water energies. Thus, the increase in potential energy upon association is mainly due to the large increase in peptide-water energy.

It is of interest to consider the hydrophobic assembly process in the context of the so-called SASA of the peptide atoms as a function of separation. SASA is commonly used for peptides and proteins as a measure of the free energy of solvating polar or nonpolar groups. Implicit solvent models (52–54) often include a term proportional to the hydrophobic or hydrophilic SASA. Examining the result in explicit solvent simulations should show how well an implicit solvent model might represent the association of the peptides. Fig. 7 shows the change in SASA relative to the value at largest separations (ΔA). The total ΔA decreases for all four peptides as the separation decreases. Although small changes in the hydrophilic SASA are apparent, Fig. 7 reveals much larger changes in hydrophobic SASA. In Fig. 8, this leads to a decrease in the fraction of hydrophobic SASA upon association of the peptides from 0.68 at large separations down to 0.65 at small separations.

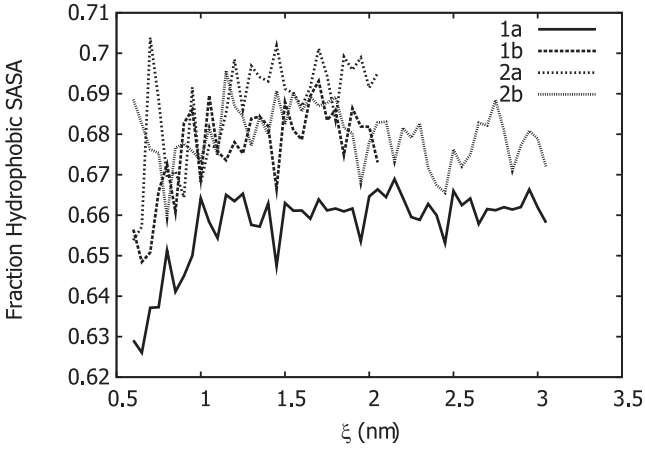

FIGURE 8 Comparison of the fraction of peptide hydrophobic SASA for each β-peptide.

The change in total SASA from large to small separation is also very similar for peptides of the same sequence. Peptides **1a** and **1b** decrease by ≈ 3 nm^2, whereas peptides **2a** and **2b** decrease by ≈ 4 nm^2. This stands in contrast to the hydrophilic SASA, which shows minimal change (<1 nm^2) at small separations. The one exception appears to be peptide **2b**, which decreases by 1 nm^2. On the other hand, the change in hydrophobic SASA is more in line with what is observed for the total SASA. Peptides **1a** and **1b** behave in a qualitatively and quantitatively similar manner, both decreasing by 2.5 nm^2. For peptide **2a**, there is a larger change in hydrophobic SASA upon aggregation (4 nm^2) than for peptide **2b** (2 nm^2). Note that at small separations we observed a change in entropy ($-T\Delta S$) of $-20\ k_BT$ for **2a** and $-10\ k_BT$ for **2b**. The factor of 2 in both $T\Delta S$ and $\Delta A_{\text{hydrophobic}}$ could indicate a relationship between the entropy and hydrophobic SASA.

The fraction of hydrophobic SASA is a function of the behavior of hydrophobic and hydrophilic SASA. Peptides **1a**, **1b**, and **2a** all show significant decreases in the fraction of hydrophobic surface area. Despite having a decrease in hydrophobic SASA, peptide **2b** shows a relatively small decrease in the fraction of hydrophobic SASA. In the associated state, peptide **1a** has the lowest fraction of hydrophobic SASA. The decrease in fraction of hydrophobic SASA is consistent with the hydrophobic driven assembly observed above.

A recent study (55) measured the forces between two linear alkanes in water using atomic force microscopy. From those measurements, a surface energy density of $\Delta G = 21$ kJ/mol/nm^2 was inferred for hydrophobic surfaces. It is of interest to compare that magnitude with the free energies calculated in this work for peptides. Fig. 7 shows a decrease of hydrophobic surface area of ~2–4 nm^2. This implies a decrease in free energy of 16.8 or 33.6 k_BT, which is too large to explain the minima of 2–5 k_BT observed in this work.

It is instructive to discuss other recent work (56,57) that has examined the organization of water confined between two hydrophobically patterned surfaces. The authors found that water forms an icelike layer between two hydrophobic surfaces (57). They also found the local water density near a hydrophobic patch surrounded by a hydrophilic surface was larger than the local water density near a completely hydrophobic surface (56). That work further emphasizes the notion that the presentation of hydrophobic and hydrophilic surfaces can have profound effects on the structure of water. It also suggests that the value of the total hydrophobic surface area needs to be understood in the context of the size of the individual patches of surface area, and that the presentation of distinct hydrophobic surfaces may have profound effects on the thermodynamics of hydrophobic association. Within that context, our work demonstrates that the sequence, particularly the facial-versus-scrambled display of hydrophilic side chains, affects the thermodynamics of peptide association. The scrambled sequence may be thought of as a hydrophobic patch surrounded by a hydrophilic surface and thus increase the local water density near the hydrophobic groups.

Another important relationship between the association of peptides and their sequence may come from the size of the hydrophobic patches. It is known that the structure of water varies with the size of hydrophobic solutes (58). Past work (58) has shown how, for the transfer of small nonpolar solutes into water, the enthalpy and entropy decrease, whereas for large nonpolar solutes, the enthalpy and entropy both increase. What occurs here may also be a manifestation of that idea: the facially amphiphilic peptides present a larger hydrophobic surface, and the nonfacially amphiphilic peptides present smaller hydrophobic patches broken up by hydrophilic patches. Changes in presentation of hydrophobic side chains affect the enthalpic and entropic terms that drive peptide association.

The number of hydrogen bonds formed between peptide-peptide, peptide-water, and water-water atoms was also determined (data not shown). Peptide-peptide hydrogen bonds were not observed in the results of all four peptides. Peptides **1a** and **1b** also exhibited no significant change in peptide-water or water-water hydrogen bonds upon association. For peptide **2a**, the number of peptide-water hydrogen bonds (ΔN_{pw}) decreased by 4, whereas the number of water-water hydrogen bonds (ΔN_{ww}) increased by the same amount. The lost peptide-water hydrogen bonds are gained by water-water hydrogen bonds, producing a neutral overall change in hydrogen bonds during peptide association. Peptide **2b** also showed a decrease of peptide-water hydrogen bonds, $\Delta N_{\text{pw}} \approx -6$. However, it was accompanied by a decrease in water-water hydrogen bonds, $\Delta N_{\text{ww}} < 0$. The larger decrease in peptide-water hydrogen bonds for peptide **2b** may be explained by the presentation of a hydrophilic residue on each face of the helix. As the peptides approach each other, they must give up some of the hydrogen bonds it would form in isolation. The lost peptide-water hydrogen bonds are not reformed by water-water or peptide-peptide hydrogen bonds.

Origins of entropy

For energy, it is possible to dissect the contributions to the potential energy to gain insights into the association process, but for the entropy it is more difficult to divide the total entropy its multiple components, including the entropy of the water and that of the peptide, which is further divided into peptide intramolecular, translational, and orientational entropy.

The entropy change of water is a result of the hydrophobic effect (59). When the hydrophobic face is exposed to the solvent, hydrogen bonds are formed within the water phase that surrounds the cavity formed by the hydrophobic side chains. Upon association of the peptides, the hydrophobic faces no longer are in contact with the water and the structure

of water decreases. Under this view, the loss of a well-defined water structure would therefore lead to an increase in entropy ($\Delta S_{water} > 0$) upon peptide association.

The second term, the peptide internal entropy, is related to the stability of the β-peptide helix itself. The secondary structure of these peptides has been shown to be particularly stable (22,23). To examine the possible effect of self-assembly on the secondary structure, we have determined the average helicity as a function of peptide separation, ξ, (Fig. 9). The average helicity of the peptides lies between 0.6 and 1.0. The helical stability indicates that, as the peptides aggregate, their conformation does not change over the separations studied here. The helicity is similar to those reported in previous work on the mechanical stability of the same four peptides (23). Our results suggest that the change in internal entropy of the peptide is negligible.

Upon association, the peptides adopt preferred orientations (Fig. 4), and the translational and configurational entropy is expected to decrease. At large separations, the peptides are not expected to exhibit a preferred orientation. The overall change in entropy (ΔS_{total}) is therefore a result of two competing contributions—a decrease in the peptide orientational and translational entropy ($\Delta S_{peptide} < 0$) and an increase in the water entropy ($\Delta S_{water} > 0$). What is interesting is that the facially amphiphilic peptides (**1a** and **2a**) both exhibit an increase in entropy ($T\Delta S$) of 10–20 k_BT. For these peptides, the magnitude of the change in water entropy is greater than the magnitude of the decrease in orientational entropy. In contrast, the isomers **1b** and **2b** exhibit small decreases or no change in the total entropy upon association, which suggests that $\Delta S_{water} \approx -\Delta S_{peptide}$.

The competition between the hydrophobic effect and peptide entropy can also be understood in light of previous results (24) in implicit solvent, in which a decrease in entropy was observed for peptide **1a**. The implicit solvent calculation captures the decrease in peptide entropy but does not explain the decrease in water entropy. As discussed in previous work with implicit and explicit solvent models with single peptides (23), the implicit model does not successfully account for the energetic and entropic interactions between two peptides. A recent study (60) highlighted the need to examine the structural details of the solvent to understand the unfolding of hydrophobic polymers in water. Hydration played an important role in the underlying thermodynamics and led to cold-induced unfolding of hydrophobic polymers in water (60).

Effect of temperature

The energetic and entropic contributions to the free energy for peptide-peptide association can be further examined by investigating the effect of temperature. For peptide **1a**, both ΔU and ΔS are positive, suggesting the counterintuitive prediction that by increasing T, the magnitude of $-T\Delta S$ would increase, w would become more negative, and the peptides would exhibit a more pronounced tendency to aggregate. This phenomenon could be viewed as cold-induced disaggregation. The first minimum of peptide **2b** near 0.8 nm would exhibit a similar response to temperature, since it also has positive ΔU and ΔS. However, the second minimum of peptide **2b** near 2.0 nm has a negative ΔU and a negative ΔS. Increasing T should therefore make $-T\Delta S$ more positive and w would become less negative (or less favorable).

To evaluate these predictions, replica exchange simulations were performed on liquid-crystalline forming peptides **1a** and **2b** as described in Model and Methods. The configuration at the free energy minima was taken as the starting configuration for replica exchange molecular dynamics simulations between 270 and 330 K. The effect of T for **1a** is shown in Fig. 10, with probability distributions of the

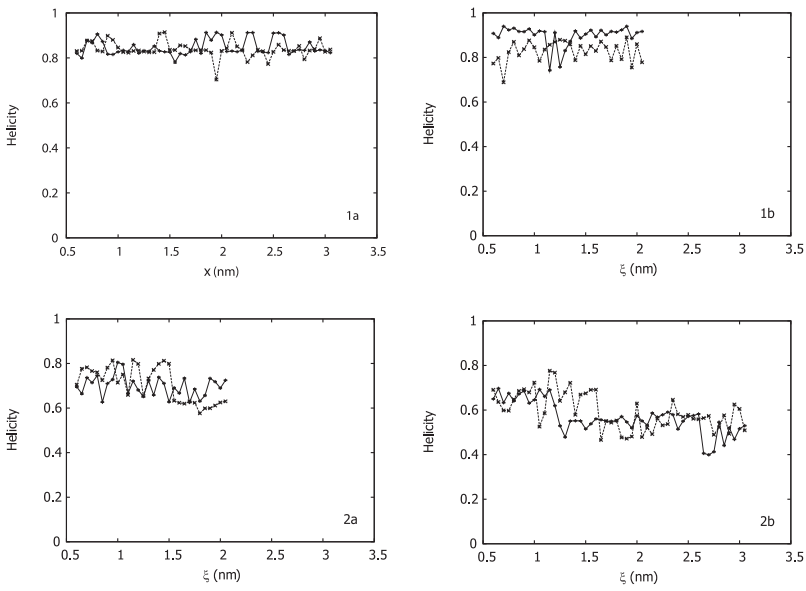

FIGURE 9 The average helicity (14-helix) as a function of peptide separation.

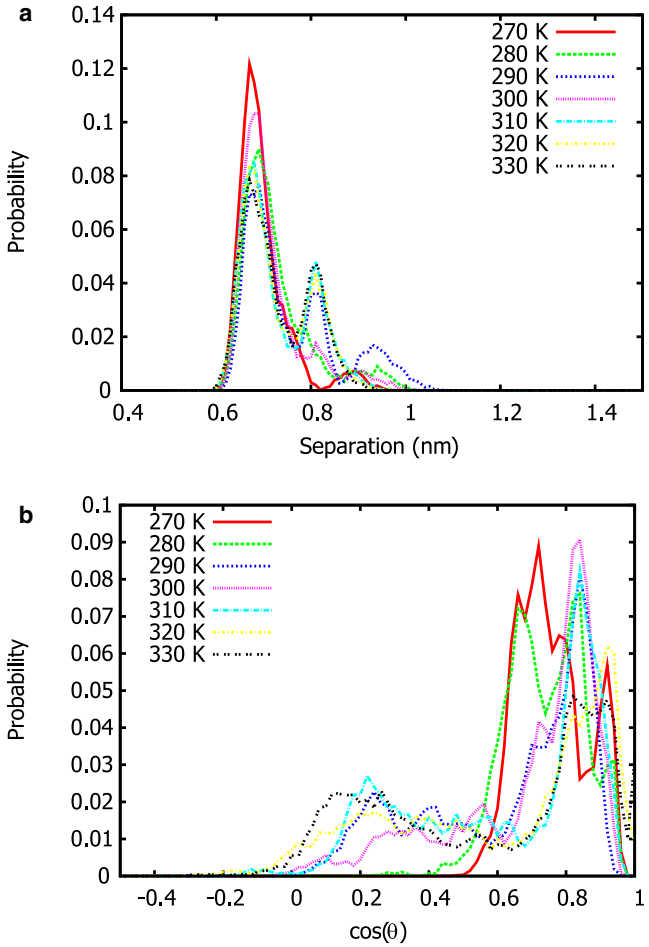

FIGURE 10 (*Color online*) The distributions of peptide separation and peptide angle (θ_1) as a function of temperature for peptide **1a**.

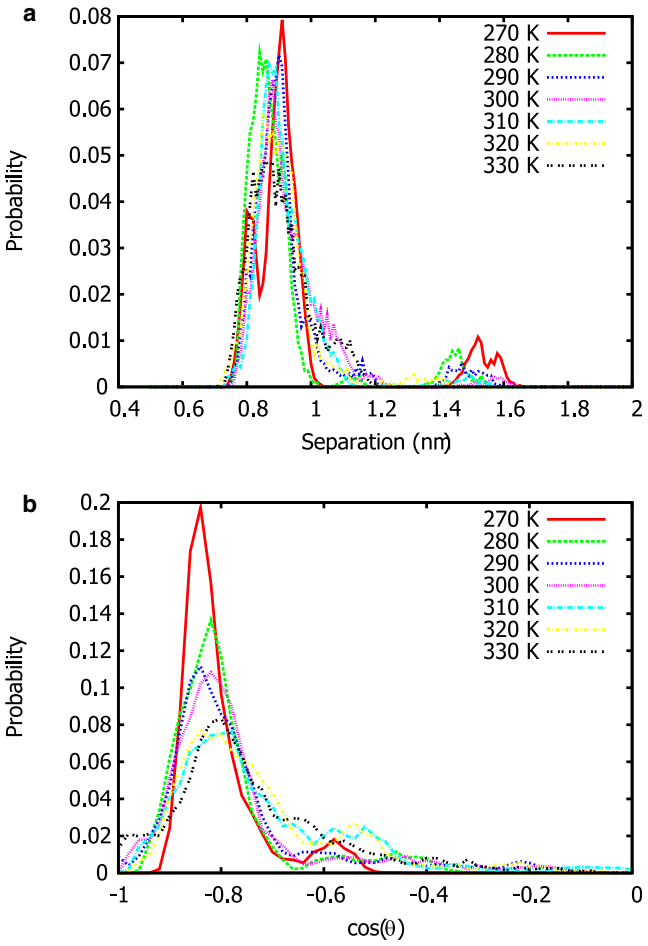

FIGURE 11 (*Color online*) The distributions of peptide separation and peptide angle (θ_1) as a function of temperature for peptide **2b** starting from 0.75 nm.

peptide separation and peptide angle. At high temperature, the peptide separation exhibits two peaks near 0.7 and 0.8 nm, whereas for lower temperatures, two peaks are observed near 0.7 and 0.9 nm. At all temperatures, the peptide separation stays within a range of 0.6–1.0 nm, suggesting that the associated state is relatively stable, even at high temperatures. The peak at the smaller distance is significantly more pronounced. The peptide angle distribution corresponds to a parallel orientation at low T, but becomes broader at higher T. In terms of the peptide orientational entropy, ΔS_{orient} becomes more negative at lower temperatures. Experimental observations (13) of peptide **1a** indicate that the liquid crystalline phase is abolished upon heating from 31° to 41°C. This is consistent with our simulations, which show that increasing T leads to a broader angle distribution. This change in the angle distribution may be responsible for the disappearance of a liquid crystalline phase.

The result for the first minimum of **2b** is shown in Fig. 11. The peptide remains in the side-by-side antiparallel arrangement from the PMF simulation. The peptide separations range from 0.7 to 1.6 nm, with distributions at lower T reaching larger separations than at higher T. This behavior is again consistent with our anticipation of cold-induced disaggregation. The peptides maintain the antiparallel arrangement, and the distribution is narrower at lower T. The angle distribution is narrower than **1a**, at all temperatures. From these simulations it can be seen that the first minimum of **2b** does not appear to be affected by high temperatures, whereas at low temperature the minimum appears to become less stable. This result is contrary to what may be expected of peptide association: that decreasing temperature should favor association. If the side-by-side association of peptide **2b** is indeed stabilized by entropy, our results suggest that lowering the temperature would cause less association of the peptides.

The result for the second minimum of **2b** is shown in Fig. 12. Both the peptide separation and peptide angle distributions are broad relative to the results for the side-by-side minima of **1a** and **2b**. Although the peptide angle distribution starts in the antiparallel orientation, it samples a broad range of antiparallel to parallel orientations. The data do not provide a clear temperature trend, but do show that this minimum near 2.0 nm is less specific than the side-by-side minimum.

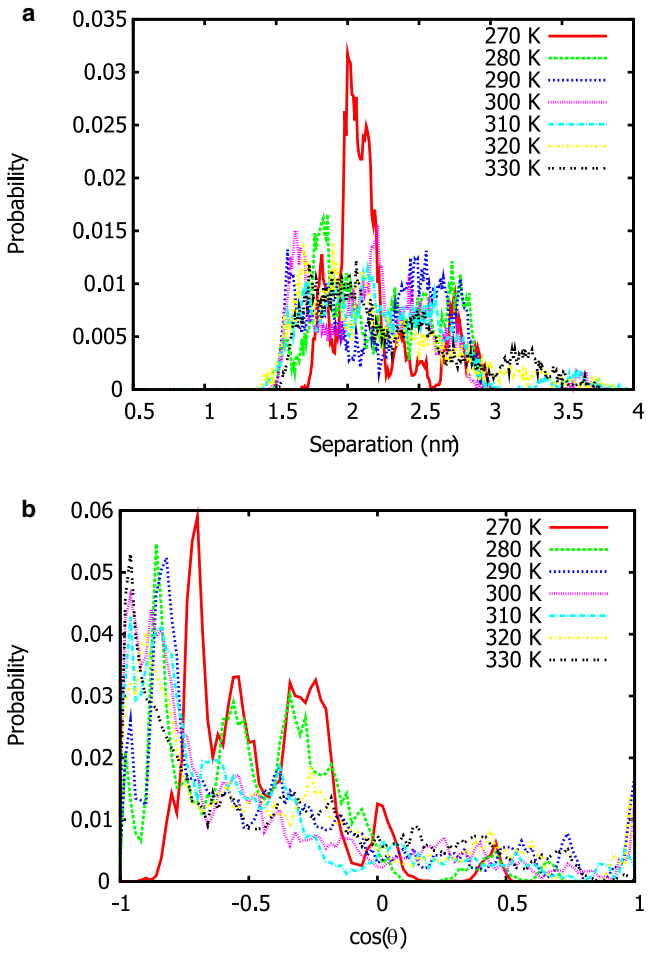

FIGURE 12 (*Color online*) The distributions of peptide separation and peptide angle (θ_1) as a function of temperature for peptide **2b** starting from 2.0 nm.

CONCLUSION

Using molecular simulations we have determined the PMF between β-peptides of different sequence and display of side chains. We have examined four different peptide sequences, each of which manifests a different association behavior in experiments. By determining the free energy of association between two peptides, we obtained minima that are consistent with experimental observations of fibers and aggregates in solution. We confirm the idea that simple changes in peptide sequence can lead to dramatic changes in aggregation, find that the peptide secondary structure is stable during association, and find that the assembly process is heavily influenced by electrostatic and hydrophobic interactions.

For peptides **1a**, **2a**, and **2b** we find evidence to support the hypothesis that the peptides assemble as a result of hydrophobic forces. The free energy minima correspond to relative orientations of the peptides in which their hydrophobic faces are buried and shielded from the water. We also find that the entropy of the system increases upon assembly, which fits with the hypothesis that the water becomes less structured when it is no longer exposed to hydrophobic atoms. Measuring the hydrophobic SASA of the peptides confirms that there is a decrease in both the absolute value and fraction of hydrophobic SASA. Further evidence for the hydrophobic assembly process is observed in the decrease of the nonbonded water-water energy and the increase in the nonbonded peptide-water energy upon association.

Peptide **1b** was not found to associate. Whereas the structure of **1a** was designed to be facially amphiphilic, **1b** contains hydrophilic residues on each face of the helix. For **1a**, the entropic term stabilizes the associated peptides while the energetic term destabilizes the associated state. For **1b**, the energetic term was also found to be largely repulsive but the entropic term did not drive association as with **1a**. The behavior of **1b** stands in contrast to **2b**, which does associate. In the case of the nonfacially amphiphilic peptide **2b**, the associated state is stabilized by energy. However, the facially amphiphilic isomer, peptide **2a**, associates because of entropy. Simple changes in the presentation of the side chains, as is the case of facial or nonfacial display of hydrophilic groups, can lead to significant changes in the entropic or energetic forces that stabilize the associated state.

Electrostatic interactions are found to play an important role. Minimization of the electrostatic terms by using more polarizable counterions, adding excess salt, or modifying the overall charge of the molecule could alter and increase considerably the tendency of the molecules to associate. Alternatively, the assembly process could be inhibited by reducing the polarity of the solvent. Changing to a less polar solvent, such as methanol, may also disrupt the hydrophobic forces that drive aggregation. Because of the favorable entropic term, another alternative to promote or hinder aggregation would be to change the temperature. By increasing the temperature, the magnitude of the entropic term would increase and could strengthen aggregation if the energetic term is constant. Conversely, a decrease in temperature may reduce the magnitude of the entropic term and reduce the strength of the aggregation. This idea was tested by replica exchange molecular dynamics simulations for two liquid crystalline forming peptides. It was found that increasing temperature leads to a decrease in association for peptide **1a**, whereas a decrease in temperature may lead to a less stable associated state for peptide **2b**.

Ongoing work involves creating coarse-grain models based on the PMF profile to examine the long-range structures that form. Atomistic simulations become increasingly expensive when one tries to examine hundreds or thousands of peptides assembling in solution. We suggest that further structural characterization of peptides **1a** and **1b** (e.g., with TEM) would add important knowledge to verifying our predictions of the PMF. Force spectroscopy experiments may also provide ways to validate our results by providing quantitative magnitudes for the forces between two peptides. By pursuing these and other studies we hope to increase our

understanding of and ability to control association of β-peptides and peptides in general.

SUPPORTING MATERIAL

The coordinate (*.crd), PDB (*.pdb), and parameter (*.psf) files for each of the four peptides studied in this work, and the force field or *.param file used for the simulation of these peptides, are available at http://www.biophysj.org/biophysj/supplemental/S0006-3495(09)00675-4.

This work is supported by the National Science Foundation through the Nanoscale Science and Engineering Center at the University of Wisconsin-Madison. The authors acknowledge the use of considerable computational resources provided through the Grid Laboratory of Wisconsin network, which is also supported by the National Science Foundation.

REFERENCES

1. Cheng, R. P., S. H. Gellman, and W. F. DeGrado. 2001. β-Peptides: from structure to function. *Chem. Rev.* 101:3219–3232.
2. Seebach, D., A. K. Beck, and D. J. Bierbaum. 2004. The world of β- and γ-peptides comprised of homologated proteinogenic amino acids and other components. *Chem. Biodivers.* 1:1111–1239.
3. Seebach, D., and J. L. Matthews. 1997. β-Peptides: a surprise at every turn. *Chem. Commun.* 1:2015–2022.
4. DeGrado, W. F., J. P. Schneider, and Y. Hamuro. 1999. The twists and turns of β-peptides. *J. Pept. Res.* 54:206–217.
5. Langenhan, J. M., and S. H. Gellman. 2004. Effects of alternative side chain pairings and reverse turn sequences on antiparallel sheet structure in β-peptide hairpins. *Org. Lett.* 6:937–940.
6. Clark, T. D., L. K. Buehler, and M. R. Ghadiri. 1998. Self-assembling cyclic β^3-peptide nanotubes as artificial transmembrane ion channels. *J. Am. Chem. Soc.* 120:651–656.
7. Raguse, T. L., J. R. Lai, P. R. Leplae, and S. H. Gellman. 2001. Toward β-peptide tertiary structure: self-association of an amphiphilic 14-helix in aqueous solution. *Org. Lett.* 3:3963–3966.
8. Martinek, T. A., I. M. Mándity, L. Fülöp, G. K. Tóth, E. Vass, et al. 2006. Effects of the alternating backbone configuration on the secondary structure and self-assembly of β-peptides. *J. Am. Chem. Soc.* 128:13539–13544.
9. Hetényi, A., I. M. Mándity, T. A. Martinek, G. K. Tóth, and F. Fülöp. 2005. Chain-length-dependent helical motifs and self-association of β-peptides with constrained side chains. *J. Am. Chem. Soc.* 127:547–553.
10. Martinek, T. A., A. Hetényi, L. Fülöp, I. M. Mándity, G. K. Tóth, et al. 2006. Secondary structure dependent self-assembly of β-peptides into nanosized fibrils and membranes. *Angew. Chem. Int. Ed.* 45:2396–2400.
11. Qiu, J. X., E. J. Petersson, E. E. Matthews, and A. Schepartz. 2006. Toward β-amino acid proteins: a cooperatively folded β-peptide quaternary structure. *J. Am. Chem. Soc.* 128:11338–11339.
12. Daniels, D. S., E. J. Petersson, J. X. Qiu, and A. Schepartz. 2007. High-resolution structure of a β-peptide bundle. *J. Am. Chem. Soc.* 129:1532–1533.
13. Pomerantz, W. C., N. L. Abbott, and S. H. Gellman. 2006. Lyotropic liquid crystals from designed helical β-peptides. *J. Am. Chem. Soc.* 128:8730–8731.
14. Pomerantz, W. C., K. D. Cadwell, Y.-J. Hsu, S. H. Gellman, and N. L. Abbott. 2007. Sequence dependent behavior of amphiphilic β-peptides on gold surfaces. *Chem. Mater.* 19:4436–4441.
15. Pomerantz, W. C., V. M. Yuwono, C. L. Pizzey, J. D. Hartgerink, N. L. Abbott, et al. 2008. Nanofibers and lyotropic liquid crystals from a class of self-assembling β-peptides. *Angew. Chem. Int. Ed.* 47:1241–1244.
16. Günther, R., H.-J. Hofmann, and K. Kuczera. 2001. Searching for periodic structures in β-peptides. *J. Phys. Chem. B.* 105:5559–5567.
17. Gee, P. J., and W. F. van Gunsteren. 2006. Terminal-group effects on the folding behavior of selected β-peptides. *Proteins. Struct. Funct. Bioinform.* 63:136–143.
18. Daura, X., W. F. van Gunsteren, and A. E. Mark. 1999. Folding-unfolding thermodynamics of a β-heptapeptide from equilibrium simulations. *Proteins Struct. Funct. Genet.* 34:269–280.
19. Daura, X., K. Gademann, H. Schäfer, B. Jaun, D. Seebach, et al. 2001. The β-peptide hairpin in solution: conformational study of a β-hexapeptide in methanol by NMR spectroscopy and MD simulation. *J. Am. Chem. Soc.* 123:2393–2404.
20. Aschi, M., A. Mollica, G. Lucente, M. P. Paradisi, and F. Mazza. 2006. Conformational properties of β-residue-containing oligopeptides in apolar solvent. *J. Mol. Struct.* 785:176–181.
21. Kritzer, J. A., J. Tirado-Rives, S. A. Hart, J. D. Lear, W. L. Jorgensen, et al. 2005. Relationship between side chain structure and 14-helix stability of β^3-peptides in water. *J. Am. Chem. Soc.* 127:167–178.
22. Rathore, N., S. H. Gellman, and J. J. de Pablo. 2006. Thermodynamic stability of β-peptide helices and the role of cyclic residues. *Biophys. J.* 91:3425–3435.
23. Miller, C. A., S. H. Gellman, N. L. Abbott, and J. J. de Pablo. 2008. Mechanical stability of helical β-peptides and a comparison of explicit and implicit solvent models. *Biophys. J.* 95:3123–3136.
24. Miller, C. A., J. P. Hernández-Ortiz, N. L. Abbott, S. H. Gellman, and J. J. de Pablo. 2008. Dipole-induced self-assembly of helical β-peptides. *J. Chem. Phys.* 129:015102.
25. Curtis, R., R. Pophale, and M. Deem. 2006. Monte Carlo simulations of the homopolypeptide pair potential of mean force. *Fluid Phase Equil.* 241:354–367.
26. Soto, P., A. Baumketner, and J.-E. Shea. 2006. Aggregation of polyalanine in a hydrophobic environment. *J. Chem. Phys.* 124:134904.
27. MacCallum, J. L., M. S. Moghaddam, H. S. Chan, and D. P. Tieleman. 2007. Hydrophobic association of α-helices, steric dewetting, and enthalpic barriers to protein folding. *Proc. Natl. Acad. Sci. USA.* 104:6206–6210.
28. Appella, D. H., J. J. Barchi, S. R. Durell, and S. H. Gellman. 1999. Formation of short, stable helices in aqueous solution by β-amino acid hexamers. *J. Am. Chem. Soc.* 121:2309–2310.
29. Raguse, T. L., J. R. Lai, and S. H. Gellman. 2003. Environment independent 14-helix formation in short β-peptides: striking a balance between shape control and functional diversity. *J. Am. Chem. Soc.* 125:5592–5593.
30. Foloppe, N., and A. D. MacKerell, Jr. 2000. All-atom empirical force field for nucleic acids: I. Parameter optimization based on small molecule and condensed phase macromolecular target data. *J. Comput. Chem.* 21:86–104.
31. MacKerell, Jr., A. D., D. Bashford, M. Bellott, R. L. Dunbrack, Jr., J. D. Evanseck, et al. 1998. All-atom empirical potential for molecular modeling and dynamics studies of proteins. *J. Phys. Chem. B.* 102:3586–3617.
32. Allen, M., and D. Tildesley. 1987. Computer Simulation of Liquids. Oxford Science Publications, Oxford, UK.
33. Frenkel, D., and B. Smith. 2002. Understanding Molecular Simulations: From Algorithms to Applications, 2nd Ed.. Academic Press, San Diego, CA.
34. Lindahl, E., B. Hess, and D. van der Spoel. 2001. GROMACS 3.0: a package for molecular simulation and trajectory analysis. *J. Mol. Model.* 7:306–317.
35. van der Spoel, D., E. Lindahl, B. Hess, G. Groenhof, A. E. Mark, et al. 2005. GROMACS: fast, flexible, and free. *J. Comput. Chem.* 26:1701–1718.
36. Berendsen, H. J. C., D. van der Spoel, and R. van Drunen. 1995. GROMACS: a message-passing parallel molecular dynamics implementation. *Comput. Phys. Commun.* 91:43–56.
37. Jorgensen, W. L., J. Chandrasekhar, J. D. Madura, R. W. Impey, and M. L. Klein. 1983. Comparison of simple potential functions for simulating liquid water. *J. Chem. Phys.* 79:926–935.

38. Essman, U., L. Perela, M. L. Berkowitz, T. Darden, H. Lee, et al. 1995. A smooth particle mesh Ewald method. *J. Chem. Phys.* 193:8577–8592.

39. Berendsen, H. J. C., J. P. M. Postma, A. DiNola, and J. R. Haak. 1984. Molecular dynamics with coupling to an external bath. *J. Chem. Phys.* 81:3684–3690.

40. Miyamoto, S., and P. A. Kollman. 1992. SETTLE: an analytical version of the SHAKE and RATTLE algorithm for rigid water models. *J. Comput. Chem.* 13:952–962.

41. Hess, B., H. Bekker, H. J. C. Berendsen, and J. G. E. M. Fraaije. 1997. LINCS: a linear constraint solver for molecular simulations. *J. Comput. Chem.* 18:1463–1472.

42. Torrie, G. M., and J. P. Valleau. 1977. Nonphysical sampling distributions in Monte Carlo free-energy estimation: umbrella sampling. *J. Comput. Phys.* 23:187–199.

43. Trzesniak, D., A.-P. E. Kunz, and W. F. van Gunsteren. 2007. A comparison of methods to compute the potential of mean force. *ChemPhysChem.* 8:162–169.

44. Kim, E. B., R. Faller, Q. Yan, N. L. Abbott, and J. J. de Pablo. 2002. Potential of mean force between a spherical particle suspended in a nematic liquid crystal and a substrate. *J. Chem. Phys.* 117:7781–7787.

45. Sugita, Y., and Y. Okamoto. 1999. Replica-exchange molecular dynamics method for protein folding. *Chem. Phys. Lett.* 314:141–151.

46. de Pablo, J. J., Q. Yan, and F. A. Escobedo. 1999. Simulation of phase transitions in fluids. *Annu. Rev. Phys. Chem.* 50:377–411.

47. Yan, Q., and J. J. de Pablo. 1999. Hyper-parallel tempering Monte Carlo: application to the Lennard-Jones fluid and the restricted primitive model. *J. Chem. Phys.* 111:9509–9516.

48. Yan, Q., and J. J. de Pablo. 2000. Hyperparallel tempering Monte Carlo simulation of polymeric systems. *J. Chem. Phys.* 113:1276–1282.

49. Faller, R., Q. Yan, and J. J. de Pablo. 2002. Multicanonical parallel tempering. *J. Chem. Phys.* 116:5419–5423.

50. Israelachvili, J. 1991. Intermolecular and Surface Force, 2nd Ed. Academic Press, San Diego, CA.

51. Geissler, P., C. Dellago, and D. Chandler. 1999. Kinetic pathways of ion pair dissociation in water. *J. Phys. Chem. B.* 103:3706–3710.

52. Feig, M., and C. L. Brooks, III. 2004. Recent advances in the development and application of implicit solvent models in biomolecule simulations. *Curr. Opin. Struct. Biol.* 14:217–224.

53. Ferrara, P., J. Apostolakis, and A. Caflisch. 2002. Evaluation of a fast implicit solvent model for molecular dynamics simulations. *Proteins Struct. Funct. Genet.* 46:24–33.

54. Guvench, O., and C. L. Brooks, III. 2004. Efficient approximate all-atom solvent accessible surface area method parameterized for folded and denatured protein conformations. *J. Comput. Chem.* 25: 1005–1014.

55. Ray, C., J. R. Brown, A. Kirkpatrick, and B. B. Akhremitchev. 2008. Pairwise interactions between linear alkanes in water measured by AFM force spectroscopy. *J. Am. Chem. Soc.* 130:10008–10018.

56. Giovambattista, N., P. G. Debenedetti, and P. J. Rossky. 2007. Hydration behavior under confinement by nanoscale surfaces with patterned hydrophobicity and hydrophilicity. *J. Phys. Chem. C.* 111: 1323–1332.

57. Giovambattista, N., P. J. Rossky, and P. G. Debenedetti. 2006. Effect of pressure on the phase behavior and structure of water confined between nanoscale hydrophobic and hydrophilic plates. *Phys. Rev. E Stat. Nonlin. Soft Matter Phys.* 73:041604.

58. Dill, K. A., T. M. Truskett, V. Vlachy, and B. Hribar-Lee. 2005. Modeling water, the hydrophobic effect, and ion solvation. *Annu Rev. Biophys. Biomol. Struct.* 34:173–199.

59. Hiemenz, P. C., and R. Rajagopalan. 1997. Principles of Colloid and Surface Chemistry, 3rd Ed.. Marcel Dekker, New York.

60. Athawale, M. V., G. Goel, T. Ghosh, T. M. Truskett, and S. Garde. 2007. Effects of length scales and attractions on the collapse of hydrophobic polymers in water. *Proc. Natl. Acad. Sci. USA.* 104:733–738.

61. Humphrey, W., A. Dalke, and K. Schulten. 1996. VMD—visual molecular dynamics. *J. Mol. Graph.* 14:33–38.